Journal of Asian Ceramic Societies 3 (2015) 271–278

HOSTED BY

Contents lists available at ScienceDirect

Journal of Asian Ceramic Societies

journal homepage: www.elsevier.com/locate/jascer

In situ synthesis and formation mechanism of ZrC and ZrB_2 by combustion synthesis from the Co-Zr-B_4C system

Mengxian Zhang [a], Yanqiu Huo [a,*], Min Huang [a], Yihang Fang [a], Binglin Zou [b,*]

[a] College of Physics and Electronic Engineering, Zhejiang Provincial Key Laboratory for Cutting Tools, Taizhou University, Taizhou 318000, China
[b] State Key Laboratory of Rare Earth Resources Utilization, Changchun Institute of Applied Chemistry, Chinese Academy of Sciences, Changchun 130022, China

ARTICLE INFO

Article history:
Received 6 March 2015
Received in revised form 1 May 2015
Accepted 19 May 2015
Available online 9 June 2015

Keywords:
ZrC-ZrB_2
Formation mechanism
Combustion synthesis

ABSTRACT

ZrC-ZrB_2-based composites were prepared by combustion synthesis (CS) reaction from 10 wt.% to 50 wt.% Co-Zr-B_4C powder mixtures. With increasing Co contents, the particle sizes of near-spherical ZrC and platelet-like ZrB_2 decreased from 1 μm to 0.5 μm and from 5 μm to 2 μm, respectively. In addition, the formation mechanism of ZrC and ZrB_2 was explored by the phase transition and microstructure evolution on the combustion wave quenched sample in combination with differential scanning calorimeter analysis. The results showed that the production of ZrC was ascribed to the solid-solid reaction between Zr and C and the precipitation from the Co-Zr-B-C melt, while ZrB_2 was prepared from the saturated liquid. The low B concentration in the Co-Zr-B-C liquid and high cooling rate during the CS process led to the presence of Co_2B and $ZrCo_3B_2$ in the composites. The addition of Co in the Co-Zr-B_4C system not only prevented ZrC and ZrB_2 particulates from growing, but also promoted the occurrence of ZrC-ZrB_2-forming reaction.

1. Introduction

ZrC and ZrB_2 have outstanding properties, such as good thermal conductivity, high melting point and excellent wear resistance. This makes them good candidates for cutting tools, reinforcing particles in composites and high temperature ceramics [1–3]. The widely used methods to produce materials combining ZrC and ZrB_2 ceramics involve a reactive hot pressing process, reactive melt infiltration, spark plasma sintering, etc. [3–7]. However, in most cases, these technologies require high temperature and complex equipment. By comparison, self-propagating high temperature synthesis (SHS), also termed as combustion synthesis (CS), is a novel processing technique currently being developed due to the low processing cost, relative simplicity of equipment and high efficiency in energy and time [8]. Thus far, this technology has been used to prepare intermetallic compounds, advanced engineering ceramics and composites.

In the past years, the combustion synthesis of TiC-TiB_2-based composites from the Ti-B_4C system with different metal additives has been extensively investigated [9–13]. Research results revealed that the incorporation of metal into Ti-B_4C powder mixtures can promote and accelerate the formation of TiC and TiB_2 by forming low melting liquid. Moreover, the addition of metal contributed to controlling the size and morphology of the resultant grains. By contrast, reports related to ZrC-ZrB_2-based composites produced by the CS route are relatively limited. These works include ZrC and ZrB_2 particles fabricated from the Al-Zr-B_4C and Cu-Zr-B_4C system, and ZrC-ZrB_2-SiC composites prepared with Zr, B_4C, Si and graphite mixtures [2,14,15]. However, the combustion synthesis of ZrC-ZrB_2-based composites from the Co-Zr-B_4C system has not been reported so far. In general, the properties of composites depend on the nature of the matrix and fillers, their proportion and interfacial binding strength as well as the distribution of the filler [16]. In comparison with Al and Cu, Co features higher Young's modulus (110–128 GPa), higher melting point (1495 °C), lower thermal expansion coefficient (13.0 μm m^{-1} K^{-1}), higher hardness (HV 1043 MPa), and lower wetting angles with ZrC (86°) and ZrB_2 (50°) [17]. Therefore, ZrC-ZrB_2/Co composites are expected to have good high temperature performance. In this paper, we explore the feasibility for the CS reaction in this system and the effect of Co addition on the resultant products. The main purpose is to investigate the formation mechanism of ZrC and ZrB_2. It is expected that these

* Corresponding author. Tel.: +86 576 88661939; fax: +86 576 88661939.
E-mail addresses: hyqhappy1199@163.com (Y. Huo), zoubinglin@ciac.ac.cn (B. Zou).
Peer review under responsibility of The Ceramic Society of Japan and the Korean Ceramic Society.

http://dx.doi.org/10.1016/j.jascer.2015.05.005

preliminary results will provide helpful guidance for the further production of ZrC-ZrB_2-based composites.

2. Experimental procedure

The starting materials were commercial powders of Co (99 wt.% purity, ~28 μm), Zr (99.5 wt.% purity, ~48 μm) and B_4C (≥95 wt.% purity, ~3.5 μm). Samples were prepared with Zr and B_4C at a ratio corresponding to the stoichiometry of ZrC-2ZrB_2 plus 10, 20, 30, 40 and 50 wt.% Co in the Co-Zr-B_4C system. The blended powders were dry mixed in a stainless steel container using ZrO_2 balls at a low speed (~50 rpm) for 8 h. Subsequently, the powder mixtures were placed in cylindrical die (22 mm in diameter) and uniaxially pressed into compacts with about 65% theoretical density. The CS experiments were performed in a stainless steel glove box full of Ar atmosphere. Briefly, the compact was placed on a 2-mm-thick graphite plate on top of a tungsten electrode. The compact was ignited by an arc heating, which was generated by passing a strong current (60 A).

The phase evolution path of the Co-Zr-B_4C system was measured by differential scanning calorimeter (DSC) (Model 200 F3 Maia, Netach, Bavaria, Germany) with the protection of flowing Ar gas (flow rate: 40 ml/min). A small amount of loose powder mixtures (~35 mg) was held in an alumina crucible and heated to a designated temperature at the heating rate of 30 °C/min. Furthermore, in the glove box full of Ar, the copper-mold-aided combustion front quenching experiment for rectangular compacts in dimensions of 65 mm × 10 mm × 2 mm was conducted.

The phase constituents of the DSC and CS products were identified by X-ray diffraction (XRD) (D/Max 2500PC Rigaku, Japan) using Cu-K_α radiation source, while the phase compositions in the different regions of the quenched sample were detected by X-ray micro-diffraction (D8 Discover with GADDS, Bruker AXS, Germany) using an 800 μm beam diameter. The microstructures of the CS and quenched specimens were examined by field emission scanning electron microscopy (FESEM) (Model S-4800, Hitachi, Tokyo, Japan) equipped with an energy-dispersive X-ray spectrometer (EDS) (Model Link-ISIS, Oxford, England).

3. Results and discussion

3.1. Thermodynamic analysis

As a preliminary analysis, the change in standard Gibbs free energy (ΔG^0) can offer information about the possible reactions, the reaction direction and extend as well as the phase stability at elevated temperatures. Hence, it is an important thermodynamic parameter for analyzing the complex reactions during the CS process. The potential chemical reactions that may take place among Co, Zr and B_4C are listed as follows:

$$\frac{4}{5}Co + \frac{1}{5}B_4C \rightarrow \frac{4}{5}CoB + \frac{1}{5}C \quad (1)$$

$$\frac{8}{9}Co + \frac{1}{9}B_4C \rightarrow \frac{4}{9}Co_2B + \frac{1}{9}C \quad (2)$$

$$\frac{1}{2}Co + \frac{1}{2}Zr \rightarrow \frac{1}{2}CoZr \quad (3)$$

$$\frac{2}{3}Co + \frac{1}{3}Zr \rightarrow \frac{1}{3}Co_2Zr \quad (4)$$

$$\frac{1}{4}B_4C + \frac{3}{4}Zr \rightarrow \frac{1}{4}ZrC + \frac{1}{2}ZrB_2 \quad (5)$$

Utilizing the thermodynamic data in Refs. [18,19], the values of ΔG^0 for Eqs. (1)–(5) were calculated, as shown in Fig. 1. It is clear that the above reactions are all thermodynamically favorable ($\Delta G^0 < 0$) in the calculated temperature ranges. It should be noted

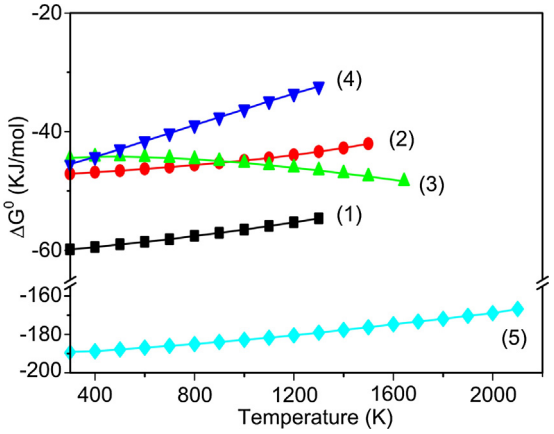

Fig. 1. Changes in ΔG^0 for reactions (1)–(5).

that the value of ΔG^0 for Eq. (5) is more negative than that of others. Thus, reaction (5) is energetically favored to proceed. Moreover, ZrC and ZrB_2 are more thermodynamically stable than cobalt zirconium and cobalt boron compounds. This suggests that if Co-Zr or/and Co-B phases are formed during the CS process, they may transform to ZrC and ZrB_2 at elevated temperatures.

3.2. DSC experiment

Thermodynamic analysis indicates that there may be complicated reactions in the Co-Zr-B_4C system. Therefore, the phase transitions for Co-B_4C, Co-Zr, Zr-B_4C and 30 wt.% Co-Zr-B_4C systems were explored by DSC, respectively. The molar ratios of Co-B_4C, Co-Zr and Zr-B_4C correspond to those in 30 wt.% Co-Zr-B_4C system, respectively. Additionally, interrupted experiments were conducted in order to make clear the reaction sequence during the heating process.

In the DSC curve of the Co-B_4C (Co/B_4C = 2.4 in molar ratio) system, no obvious endothermic or exothermic peaks were observed (Fig. 2a). Heating the mixtures to 600 °C, only Co and B_4C were found in the DSC products (Fig. 3a). For the reactant quenched at 800 °C, a large amount of Co_2B was determined by XRD (Fig. 3b). This means that the solid-state reaction of $Co + B_4C \rightarrow Co_2B + C$ mainly took place in the temperature range of 600–800 °C. When the temperature ranged from 800 °C to 1000 °C, Co-B_4C reaction was further activated. It gave rise to the significant enhancement

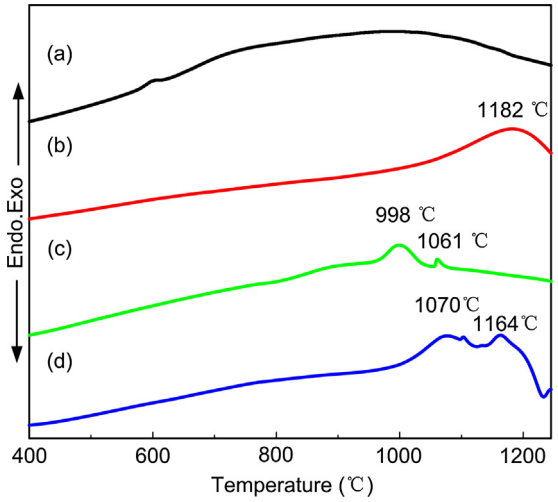

Fig. 2. DSC curves of the (a) Co-B_4C, (b) Zr-B_4C, (c) Co-Zr and (d) 30 wt.% Co-Zr-B_4C powder mixtures, respectively.

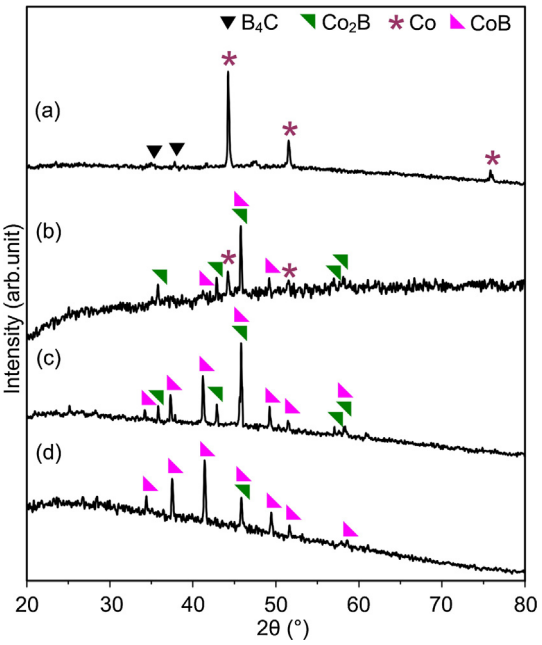

Fig. 3. XRD patterns for the DSC products of the Co-B_4C system quenched at (a) 600 °C, (b) 800 °C, (c) 1000 °C and (d) 1250 °C, respectively.

of CoB peaks and the disappearance of Co (Fig. 3c). According to the calculated results in Fig. 1, the values of ΔG^0 for Eqs. (1) and (2) are negative. Thus, the fabrication of Co_2B and CoB is thermodynamically feasible. With further increasing temperature, Co_2B reacted with B_4C to form CoB. As a result, Co_2B content decreased, while CoB content increased in the final products (Fig. 3d). It is worth noting that C peaks were not identified by XRD, though C atoms should be set free from above reactions. It may be owing to the amorphous structure of C.

In the DSC curve of the Zr-B_4C (Zr/B_4C = 3 in molar ratio) system, only an exothermic peak is present at temperature close to 1182 °C (Fig. 2b). Besides Zr and B_4C phases, a great number of ZrC and ZrB_2 were found in the final products (Fig. 4b). Clearly, this exothermic event was caused by ZrC-ZrB_2-forming reaction between Zr and B_4C particles. Guo et al. [4] produced ZrB_2-ZrC-Zr cermets with Zr and B_4C powder mixtures by reactive hot pressing. They found that for samples sintered at 900 °C or above, Zr and B_4C mixtures can be converted into ZrB_2 and ZrC. It is notable that the diffraction peak of B_4C is far weaker than Zr or it cannot be detected though the mole percentages of B_4C and Zr are 25% and 75%, respectively. Similar phenomena also existed in the Cu-B_4C [20] and Co-B_4C systems.

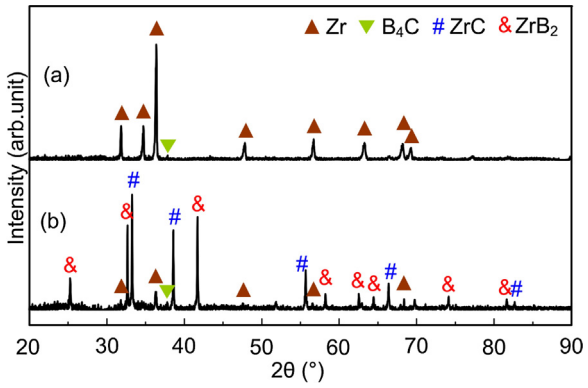

Fig. 4. XRD patterns for the DSC products of the Zr-B_4C system quenched at (a) 900 °C and (b) 1250 °C, respectively.

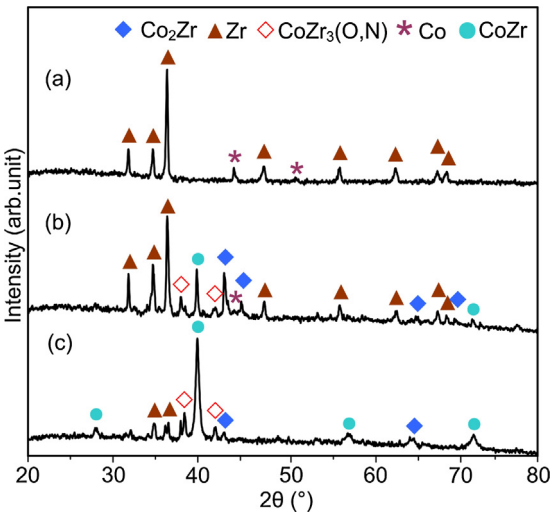

Fig. 5. XRD patterns for the DSC products of the Co-Zr system quenched at (a) 800 °C, (b) 998 °C and (c) 1250 °C, respectively.

The relative diffraction intensity formula of phase in the powder mixtures can be described as follows:

$$I_P = n \cdot |F|^2 \cdot \frac{1+\cos^2 2\theta}{\sin^2\theta\cos\theta} \cdot e^{-2M} \quad (6)$$

where n, F, $\frac{1+\cos^2 2\theta}{\sin^2\theta\cos\theta}$, θ and e^{-2M} are multiple factor, structure factor, angle factor, Bragg angle and temperature factor, respectively. F is the scattering power of unit cell and is connected with the atomic characteristics and location in the unit cell. Therefore, the weak

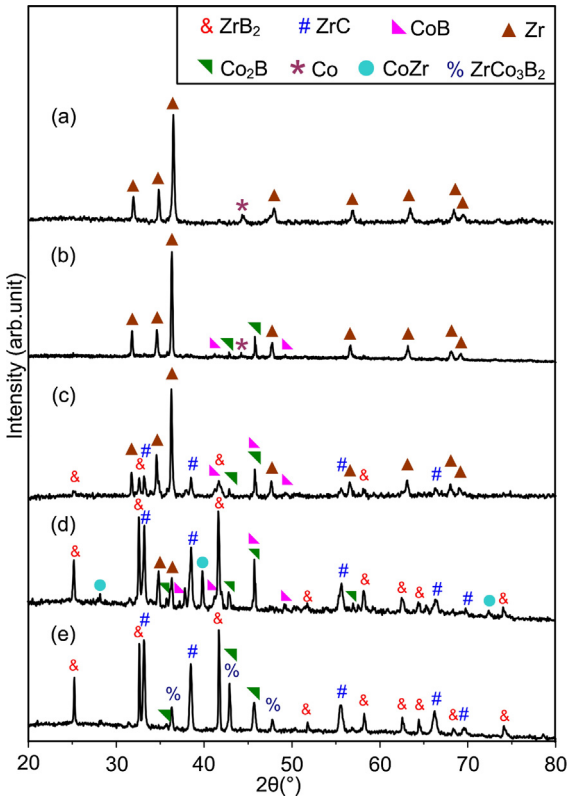

Fig. 6. XRD patterns of (a) 30 wt.% Co-Zr-B_4C powder mixtures and corresponding DSC products quenched at (b) 1000 °C, (c) 1070 °C, (d) 1164 °C and (e) 1250 °C, respectively.

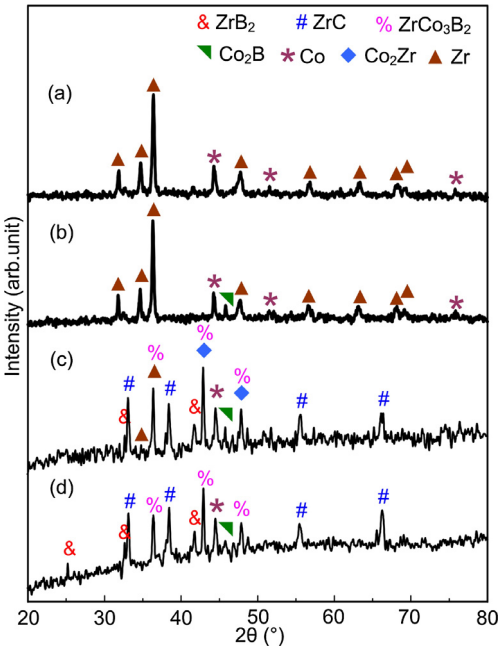

Fig. 7. X-ray micro-diffraction patterns of the quenched sample in the (a) unreacted region, (b) preheated region, (c) reacting reaction and (d) fully reacted region, respectively.

or absent B_4C peaks in the mixtures are possibly on account of its atomic characteristics and crystalline lattice.

In the DSC curve of the Co-Zr (Co/Zr = 0.8 in molar ratio) system (Fig. 2c), there are two exothermic peaks at about 998 °C and 1061 °C, respectively. Heating Co-Zr mixtures to 800 °C, no reactions occurred in accordance to the XRD patterns in Fig. 5a. With increasing temperature, Zr reacted with Co to form CoZr and Co_2Zr compounds, which gave rise to the exothermic peak at 998 °C. Thus, new phases Co_2Zr and CoZr appeared in the DSC products (Fig. 5b). The reason for the presence of $CoZr_3(O, N)$ phase may be owing to the invasion of atmosphere during the heating period. In the light of the thermodynamic analysis in Fig. 1, the synthesis of Co_2Zr and CoZr through Co-Zr reaction is theoretically feasible. As the temperature was raised to 1061 °C, the reaction of $Zr + Co_2Zr \rightarrow CoZr$ took place. Consequently, the diffraction peaks of CoZr became intensive, while those of Co_2Zr and Zr became weak in the final products (Fig. 5c).

The DSC curve of 30 wt.% Co-Zr-B_4C system includes two obvious exothermic peaks at around 1070 °C and 1164 °C, respectively (Fig. 2d). For the reactants quenched at 1000 °C, a small number of Co_2B and CoB compounds were detected by XRD (Fig. 6b). This implies that the reaction of $Co + B_4C \rightarrow Co_yB + C$ ($y = 1, 2$) occurred. The phenomenon was also observed in the DSC experiments of the Co-B_4C system. However, no Co-Zr compounds were formed at 1000 °C as compared with DSC results of the Cu-Zr system. Research on the reaction process of the Cu-Zr-B_4C system indicated that the

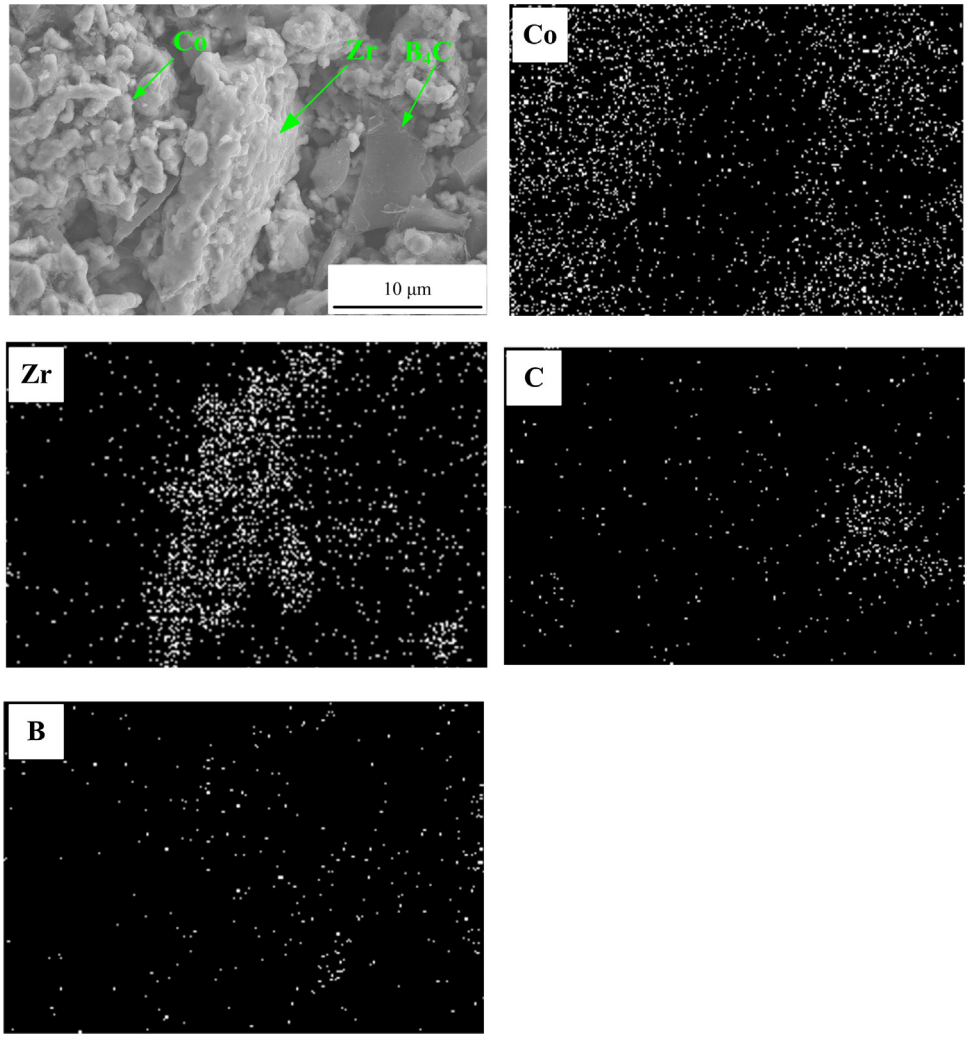

Fig. 8. Microstructure and elemental mapping micrographs in the unreacted region.

presence of B_4C particles may restrain solid-state reaction between Cu and Zr powders [15]. It is inferred that the B_4C in the Co-Zr-B_4C system played the same role. Without no doubt, B_4C can decrease the contact surface and extend diffusion distance between Co and Zr particulates, which is unfavorable to the formation of Co-Zr compounds. In addition, it can be concluded that Cu-B_4C reaction is more favorable than Co-Zr reaction. It is possibly due to the fine B_4C particles and large contact surface between Co and B_4C powders.

Heating the reactant to 1070 °C, new phases ZrC and ZrB_2 were identified in the DSC products (Fig. 6c). So, this exothermic peak mainly resulted from the formation of ZrC and ZrB_2. After the solid-solid reaction between Co and B_4C, C atoms were set free. Then, the free C atoms reacted with Zr to form ZrC. The ZrC-forming reaction is exothermic, which would improve the reactivity of the surrounding particles. As a consequence, the reaction of $Zr + B_4C \rightarrow ZrC + ZrB_2$ was induced. These two reactions were put together and led to the exothermic peak with the maximum temperature at 1070 °C, and the stronger diffraction intensity of ZrC peaks in comparison with that of ZrB_2 peaks (Fig. 6c). The forming temperature of ZrC and ZrB_2 (1070 °C) in 30 wt.% Co-Zr-B_4C system is lower than that in the Zr-B_4C system (1182 °C). Therefore, it is accepted that the addition of Co to the Zr-B_4C mixtures promotes the formation of ZrC and ZrB_2.

Increasing temperature brought about the second exothermic peak at approximately 1164 °C. In the DSC products, new phase CoZr was detected (Fig. 6d). Furthermore, the diffraction peaks of ZrC and ZrB_2 were much stronger than those in Fig. 6c. As we know, high temperature favors atomic diffusion. Hence, the diffusion rate of Co and Zr increased as the temperature was raised to 1164 °C. Spontaneously, the solid-state reaction between Co and Zr to form CoZr proceeded. Referring to the DSC analysis in the Co-Zr system, the formation of CoZr will release heat and elevate the temperature around. Consequently, the reaction of $Zr + B_4C \rightarrow ZrC + ZrB_2$ was triggered. Once again, ZrC-ZrB_2-forming reaction (1164 °C) was accelerated as compared with that in the Zr-B_4C system (1182 °C).

In the temperature range of 1164–1250 °C, no obvious exothermic peaks were observed. However, CoB, CoZr and Zr disappeared, while $ZrCo_3B_2$ phase appeared in the final products (Fig. 6e). On the basis of the DSC analysis, the phase evolution in 30 wt.% Co-Zr-B_4C system can be described as: (1) $Co + Zr + B_4C \rightarrow$ (2) $Co + Zr + B_4C + Co_yB + C \rightarrow$ (3) $Co + Zr + B_4C + Co_yB + ZrC \rightarrow$ (4) $Co + Zr + B_4C + Co_yB + ZrC + ZrB_2 \rightarrow$ (5) $Co + Zr + B_4C + Co_yB + ZrC + ZrB_2 + CoZr \rightarrow$ (6) $ZrC + ZrB_2 + Co_2B + ZrCo_3B_2$.

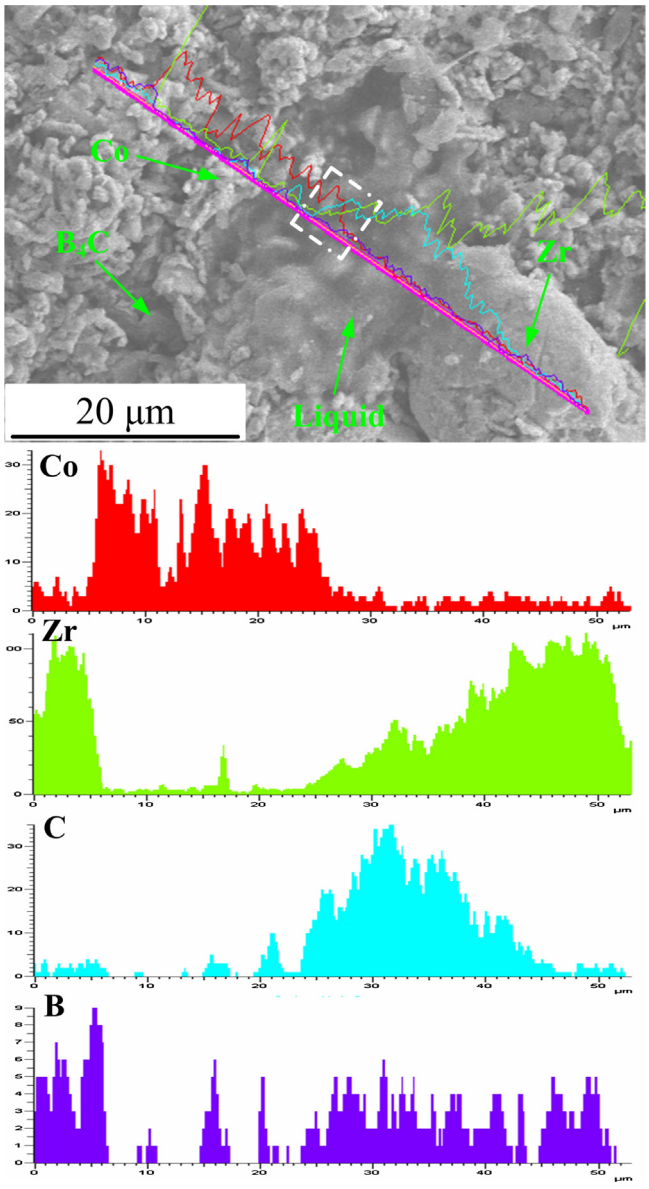

Fig. 9. Microstructure and elemental scanning spectra in the reacting region.

3.3. *Combustion wave quenching experiments*

DSC analysis contributes to understanding the formation path of ZrC and ZrB_2 in the Co-Zr-B_4C system. However, it may not be fully reliable for the different experimental conditions between the DSC and CS process. For instance, CS reaction was ignited by heating one end of the reactant, while DSC reaction was triggered by heating the whole reactant [8]. In order to further make clear the formation mechanism of ZrC and ZrB_2, it is necessary to quench the combustion wave during its passage through the sample. The combustion wave quenching experiments succeeded in 50 wt.% Co-Zr-B_4C specimen with 1-μm Co, 48-μm Zr and 3.5-μm B_4C particles. The quenched sample could be roughly divided into four regions along the propagation direction of combustion wave front, i.e. unreacted region, preheated region, reacting region and fully reacted region. From the X-ray micro-diffraction results in the different regions (Fig. 7), it can be seen that the phase constituents gradually changed.

In the unreacted region, there exist only Co and Zr phases, without any intermediates (Fig. 7a). This suggests that the powder mixtures were not affected by the heat generated from the combustion front. Microstructure observation and energy spectrum analysis in this region (Fig. 8) shows that the fine white particles are Co, the large white ones represent Zr and the fine gray grains are B_4C. Compared with the unreacted region, Co_2B phase was formed in the preheated region (Fig. 7b). The appearance of Co_2B should be Co-B_4C reaction triggered by the heat generated from the reacting region. DSC results also indicated that the solid-solid reaction between Co and B_4C initially took place in the Co-Zr-B_4C system (Fig. 6a).

Fig. 7c is the XRD patterns in the reacting region. As seen, new phases ZrC, ZrB_2, Co_2Zr and $ZrCo_3B_2$ appeared. After Co-B_4C reaction, the free C atoms reacted with Zr particles to form ZrC, which will elevate temperature around. Thus, the diffusion rate of Co and Zr increased, and the solid-solid reaction of $Co + Zr \rightarrow Co_2Zr$ happened. Li et al. [21] found that the synthesis of ZrC with Zr and C powders can bring about the evaporation of NaCl (boiling point: 1413 °C). It is inferred that ZrC-forming reaction also promoted the melting of Co_2B (melting point: 1280 °C) at the local area. Subsequently, Co, Zr and B_4C gradually dissolved and diffused into the melt to form Co-Zr-B-C liquid because of the capillary penetration and the increasing diffusion path of liquid. Fig. 9 is the

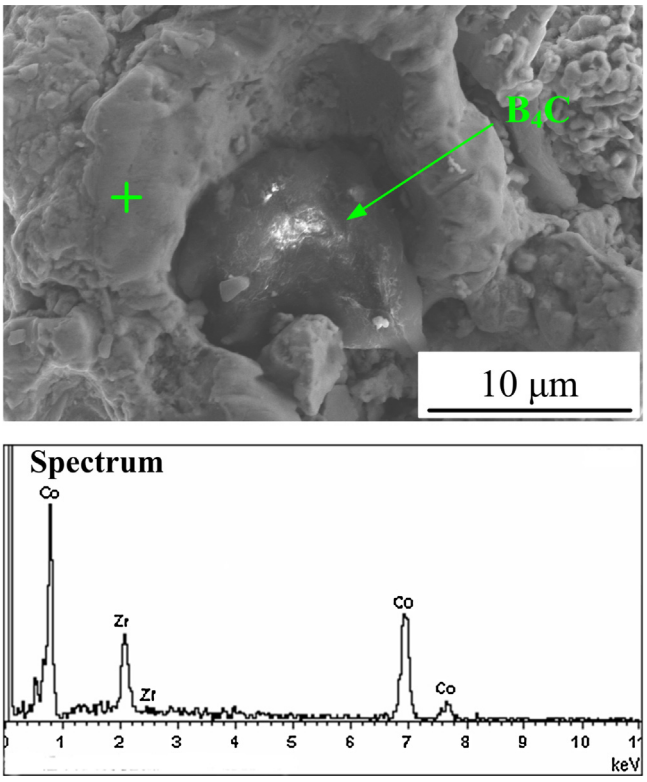

Fig. 10. Microstructure and the EDS spectra of corresponding dot in the reacting region close to the fully reacted region.

microstructure in the reacting region. A molten-like phase can be observed. According to the EDS-line analysis, the molten-like phase was made of Co, Zr, B and C elements. This indicated that Co-Zr-B-C liquid was formed in the reacting region. Generally, atoms in the liquid are able to move more freely, and they are much more likely to collide and react with one another. As a consequence, ZrC-ZrB_2-forming reaction was promoted. Once the more stable ZrC and ZrB_2 in the liquid became saturated, they were precipitated. Liang et al. [9] explored the reaction path of TiC and TiB_2 in 20 wt.% Cu-Ti-B_4C system. They found that in the Ti-B_4C system, TiC and TiB_2 were synthesized at 1093 °C through the solid-solid reaction between Ti and B_4C. While in 20 wt.% Cu-Ti-B_4C system, TiC-TiB_2-forming temperature was reduced to 990 °C due to the formation of Cu-Ti-B-C liquid. It should be noted that the location of the region containing Co does not quite correspond to those containing Zr, C, and B, as seen in the EDS-line analysis in Fig. 9. As we know, diffusion is a time-dependent process and usually goes from regions of higher concentration to regions of lower concentration. So in the melt, Co concentration close to Co particles was higher than that away from Co particles, and gradually decreased from the left to the right. Similar behavior also existed in the concentration variation of Zr. At the center (white-lined box in Fig. 9), Co, Zr and C were simultaneously detected owing to a short distance to the surrounding particles. Moreover, B concentration in the liquid was relatively low. The EDS technique measures X-rays emitted from the sample during bombardment by an electron beam to characterize the elemental composition [22]. However, light elements (e.g. B) are difficult to detect for the low fluorescence quantum yield and low X-ray energy as well as strong absorption. In Fig. 8, B "counts" are few as well. On the other hand, the diffusion of C away from the B_4C is much faster than that of B [23]. These may lead to the low intensity of B in the liquid.

Fig. 10 is the microstructure in the reacting region close to the fully reacted region. In Fig. 10, a molten-like phase including Co and

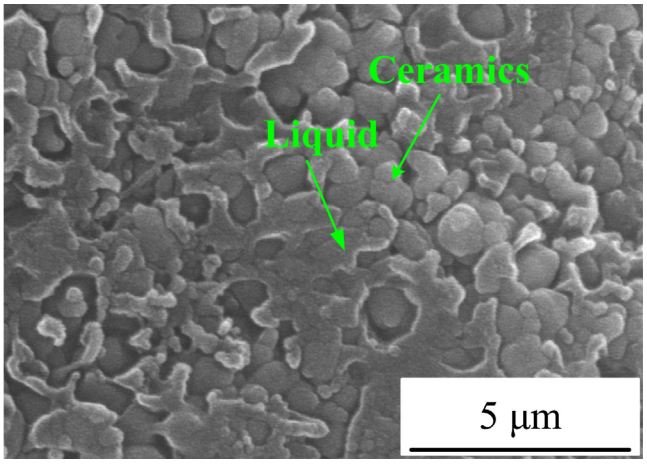

Fig. 11. Microstructure in the fully reacted region.

Zr elements was observed. It is speculated that the formation of ZrC and ZrB_2 will release heat and result in the melting of Co_2Zr. After the dissolution and diffusion of B_4C into Co-Zr melt, more Co-Zr-B-C liquid was formed. In this way, Co_2Zr promoted ZrC-ZrB_2-formation reaction.

Fig. 11 is the microstructure in the fully reacted region, which further offers evidence that ZrC and ZrB_2 were precipitated from the liquid. The phase compositions in this region (Fig. 7d) are similar with those in the CS products with 50 wt.% Co content (Fig. 12e). Besides the desired Co, ZrC and ZrB_2 phases, Co_2B and $ZrCo_3B_2$ compounds were determined by XRD. Makino et al. [24] considered that the presence of nonequilibrium structures was because of the high cooling rate and high defect concentration during the CS processes. According to the EDS line in Fig. 9, C concentration in the

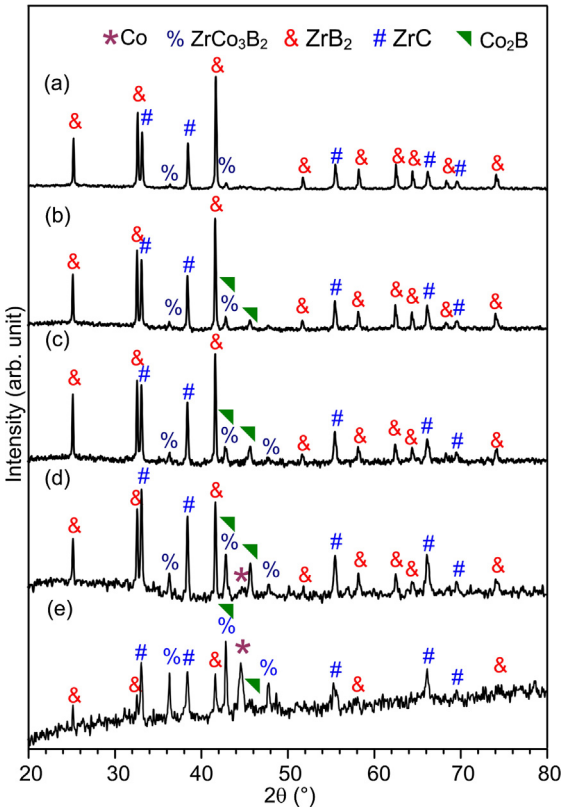

Fig. 12. XRD patterns for the CS products with (a) 10 wt.%, (b) 20 wt.%, (c) 30 wt.%, (d) 40 wt.% and (e) 50 wt.% Co contents, respectively.

Co-Zr-B-C liquid is higher than B concentration because the diffusion of C away from the B_4C is much faster than that of B [23]. Moreover, ZrC is a substoichiometric phase in the light of Zr-C phase diagram [25]. Therefore, the formation of ZrC may consume more Zr owing to the high C concentration. Accordingly, there were insufficient Zr atoms to produce ZrB_2 and redundant B atoms in the liquid. So, with the precipitation of ZrC and ZrB_2, Co, Co_2B and $ZrCo_3B_2$ crystallized from the liquid.

Based on the above observation and analysis, we believed that the formation route of ZrC and ZrB_2 during the CS process experienced the following reactions:

$$Co(s) + B_4C(s) \rightarrow Co_yB(s) + C(s) \quad (7)$$

$$Zr(s) + C(s) \rightarrow ZrC(s) \quad (8)$$

$$Co(s) + Zr(s) \rightarrow Co_xZr(s) \quad (9)$$

$$Co_yB(s) \rightarrow Co\text{-}B(l) \quad (10)$$

$$Co\text{-}B(l) + Co(s) + Zr(s) + B_4C(s) \rightarrow Co\text{-}Zr\text{-}B\text{-}C(l) \quad (11)$$

$$Co\text{-}Zr\text{-}B\text{-}C(l) \rightarrow ZrC(s) + ZrB_2(s) + Liquid \quad (12)$$

$$Co_2Zr(s) \rightarrow Co\text{-}Zr(l) \quad (13)$$

$$Co\text{-}Zr(l) + B_4C(s) \rightarrow ZrC(s) + ZrB_2(s) + Liquid \quad (14)$$

$$Liquid \rightarrow Co(s) + Co_2B(s) + ZrCo_3B_2(s) \quad (15)$$

3.4. Phases and microstructures of CS products

Fig. 12 is the typical XRD patterns of the CS products with Co contents ranging from 10 wt.% to 50 wt.%. As indicated, besides the expected ZrC, ZrB_2 or/and Co phases, a small number of Co_2B and $ZrCo_3B_2$ compounds were determined. This implies that the combustion synthesis of ZrC-ZrB_2-based composites from the Co-Zr-B_4C system is feasible. As mentioned before, the appearance of Co_2B or/and $ZrCo_3B_2$ is due to the high defect concentration of B and high cooling rate during the CS processes. Therefore, increasing B concentration in the Co-Zr-B-C liquid may restrain the presence of Co_2B or/and $ZrCo_3B_2$ in the CS products. In a previous work [20], the effect of B_4C particle size on the CS process and product in the Cu-Zr-B_4C system was investigated. Research results showed that increasing B_4C size will reduce the dissolution rate of B_4C in Cu-Zr liquid and lead to the incomplete conversion of ZrC and ZrB_2. It is deduced that using finer B_4C particles may increase the dissolution rate of B_4C and B concentration in the liquid, and thus refrain the

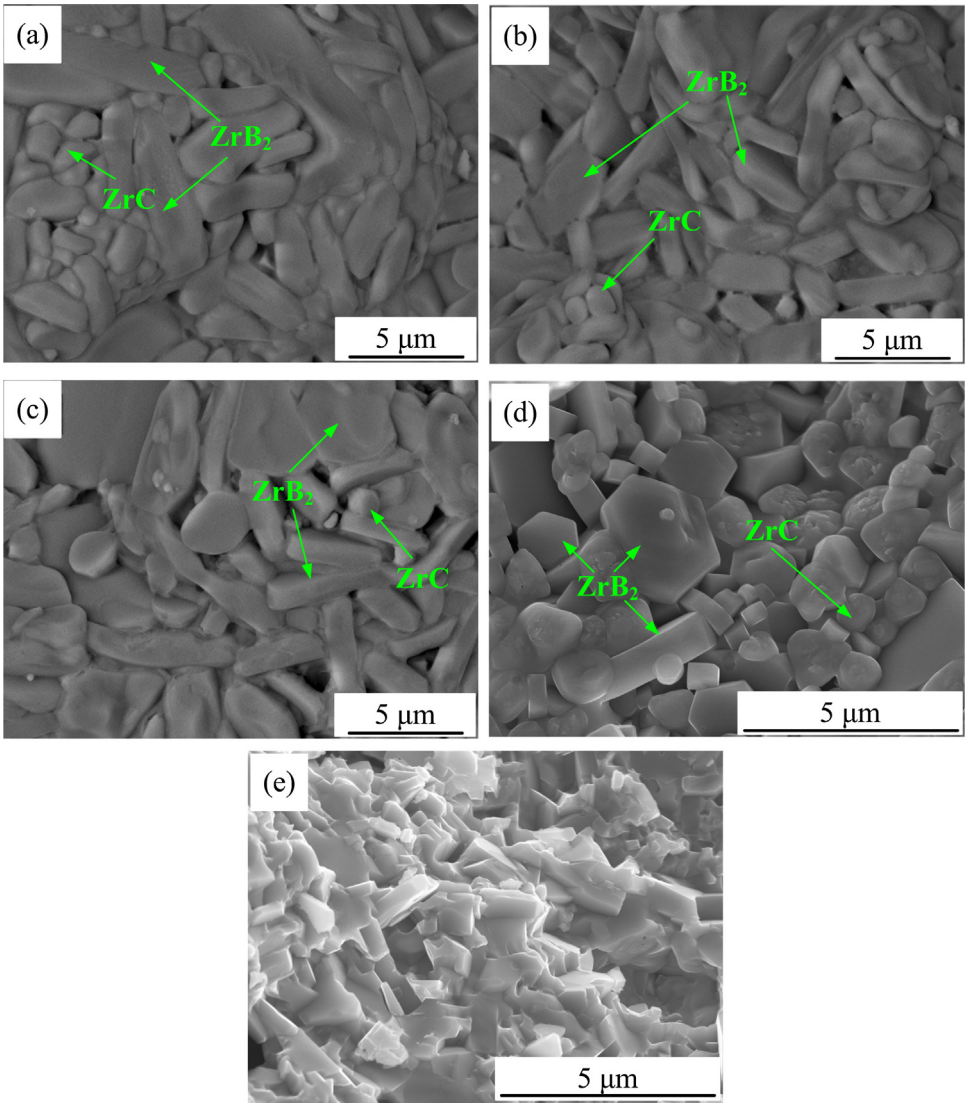

Fig. 13. Microstructures for the CS products with (a) 10 wt.%, (b) 20 wt.%, (c) 30 wt.%, (d) 40 wt.% and (e) 50 wt.% Co contents, respectively.

production of Co_2B or/and $ZrCo_3B_2$. However, relevant experiments have not been conducted for the lack of fine B_4C.

Fig. 13 shows the morphologies of ZrC and ZrB_2 in the CS products. It can be observed that ZrC and ZrB_2 grains displayed close to spherical [26] and platelet-like morphologies [4,27], respectively. Furthermore, with increasing Co contents, the particle size of ZrC decreased from about 1 μm to 0.5 μm, while ZrB_2 size was reduced from about 5 μm to 2 μm. Referring to Fig. 12, increasing Co contents will result in the reduction of ZrC and ZrB_2 and the enhancement of Co in the CS products. On one hand, the cooling rate increased for the higher thermal conductivity coefficient of metal. Correspondingly, the dwell time of the final products at elevated temperature was shorted. This prevented the growth of ZrC and ZrB_2. On the other hand, the heat released from ZrC-ZrB_2-froming reaction decreased. Spontaneously, the combustion temperature decreased. It brought about the reduction in the size of resultant ZrC and ZrB_2 because the growth of grains is an exponential function of the temperature [11]. Moreover, the increase of liquid metal surrounding ceramic particles gives rise to the increased diffusion path, and prevents the ceramic particles to form larger particles [13]. Increasing Co contents in the Co-Zr-B_4C system will promote the formation of Co-B and Co-Zr compounds. Correspondingly, more Co-Zr-B-C liquid will be formed according to the analysis on the combustion wave quenching experiments. As a result, the sizes of ZrC and ZrB_2 particles turned to be smaller with increasing Co contents.

4. Conclusions

(1) ZrC-ZrB_2-based composites were produced by way of CS method from the Co-Zr-B_4C system.
(2) With increasing Co contents, the particle size of ZrC and ZrB_2 reduced.
(3) The addition of Co to Zr-B_4C mixtures promoted the formation of ZrC and ZrB_2.
(4) ZrB_2 was prepared from Co-Zr-B-C liquid, while ZrC was produced by the solid-solid reaction between Zr and C and the precipitation from the saturated liquid.

Acknowledgements

This work is supported by National Natural Science Foundation of China (No. 51404517, No. 51101143 and No. 51472235), Natural Science Foundation of Zhejiang Province (No. LQ15E010002) and Open Foundation of Zhejiang Provincial Key Laboratory for Cutting Tools (No. ZD201307).

References

[1] Y.Y. Li, Q.G. Li, Z. Wang, C. Wu, G.P. Shi and M.J. Liu, J. Asian Ceram. Soc., 3, 1–15 (2015).
[2] R. Licheri, R. Orrù, C. Musa and G. Cao, Mater. Lett., 62, 432–435 (2008).
[3] L. Xu, C.Z. Huang, H.L. Liu, B. Zou, H.T. Zhu, G.L. Zhao and J. Wang, Int. J. Refract. Met. Hard Mater., 37, 98–105 (2013).
[4] S.Q. Guo, Ceram. Int., 40, 12693–12702 (2014).
[5] S.A. Chen, C.R. Zhang, Y.D. Zhang and H.F. Hu, Composites Part B: Eng., 60, 222–226 (2014).
[6] F. Goutier, G. Trolliard, S. Valette, A. Maître and C. Estournes, J. Eur. Ceram. Soc., 28, 671–678 (2008).
[7] D.S. King, G.E. Hilmas and W.G. Fahrenholtz, J. Eur. Ceram. Soc., 34, 3549–3557 (2014).
[8] J.J. Moore and H.J. Feng, Prog. Mater. Sci., 39, 243–273 (1995).
[9] Y.H. Liang, H.Y. Wang, Y.F. Yang, Y.L. Du and Q.C. Jiang, Int. J. Refract. Met. Hard Mater., 26, 383–388 (2008).
[10] X.G. Huang, Z.M. Zhao, L. Zhang, C. Yin and J.Y. Wu, J. Asian Ceram. Soc., 2, 144–149 (2014).
[11] B.L. Zou, J.Y. Xu, Y. Wang, S.M. Zhao, X.Z. Fan, Y. Hui, X. Zhou, W.Z. Huang, X.L. Cai, S.Y. Tao, H.M. Ma and X.Q. Cao, Chem. Eng. J., 233, 138–148 (2013).
[12] B. Aminikia, Powder Technol., 232, 78–86 (2012).
[13] Y.F. Yang, H.W. Wang, R.Y. Zhao, Y.H. Liang and Q.C. Jiang, Int. J. Refract. Met. Hard Mater., 26, 77–83 (2008).
[14] Q.D. Hu, P. Luo, M.X. Zhang, M.S. Song and J.G. Li, Int. J. Refract. Met. Hard Mater., 31, 89–95 (2012).
[15] M.X. Zhang, Y.Q. Huo, Q.D. Hu, P. Zhang and B.L. Zou, Int. J. Refract. Met. Hard Mater., 43, 102–108 (2014).
[16] S. Poovarodom, D. Hosseinpour and J.C. Berg, Ind. Eng. Chem. Res., 47, 2623–2629 (2008).
[17] G.A. Yasiskaya, Powder Metall. Met. Ceram., 5, 557–559 (1966).
[18] D.L. Ye and J.H. Hu, Notebook of Thermodynamic Data of Inorganic, second ed., Metallurgical Industry Press, Beijing (2002).
[19] A. Durga and K.C. Hari Kumar, Calphad, 34, 200–205 (2010).
[20] M.X. Zhang, Y.Q. Huo, M. Huang, Y.H. Fang and G.P. Wang, J. Asian Ceram. Soc., 3, 38–43 (2015).
[21] J. Li, Z.Y. Fu, W.M. Wang, H. Wang, L. Soowohn and N. Kochi, J. Chin. Ceram. Soc., 38, 979–985 (2010).
[22] L.D. Hanke, Handbook of Analytical Methods for Materials, Materials Evaluation and Engineering, Plymouth (2001).
[23] P. Shen, B.L. Zou, S.B. Jin and Q.C. Jiang, Mater. Sci. Eng. A, 454–455, 300–309 (2007).
[24] A. Makino and C.K. Low, J. Am. Ceram. Soc., 77, 778–786 (1994).
[25] T.B. Massalski, H. Okamoto, P.R. Subramanian and L. Kacprzak, Binary Alloy Phase Diagrams, second ed., ASM International Materials Park, Ohio (1990).
[26] M.X. Zhang, B. Huang, Q.D. Hu and J.G. Li, Int. J. Refract. Met. Hard Mater., 31, 230–235 (2012).
[27] H.T. Liu, J. Zou, D.W. Ni, W.W. Wu, Y.M. Kan and G.J. Zhang, Scr. Mater., 65, 37–40 (2011).